Journal of Solid Mechanics Vol. 16, No. 1 (2024) pp. 48-64
DOI: 10.60664/jsm.2024.3111794

Research Paper

Free Vibration Analysis of A Sandwich Cylindrical Shell with A Functionally Graded Auxetic Honeycomb Core via The zig-zag Theory

H. Amirabadi *

Department of Mechanical Engineering, Abadeh Branch, Islamic Azad University, Abadeh, Iran

Received 16 November 2023; Received in revised form 29 June 2024; Accepted 2 July 2024

ABSTRACT

In the present paper, a semi-analytical solution is presented for the free vibration analysis of a sandwich cylindrical shell with a re-entrant auxetic honeycomb (AH) core fabricated from metal-ceramic functionally graded materials (FGM). It is assumed that the volume fraction of the ceramic phase in the functionally graded auxetic honeycomb (FGAH) core increases from zero at the inner surface of the core to one at the outer one according to various patterns including power-law function (P-FGM), sigmoid function (S-FGM), and exponential function (E-FGM). The FGAH core is covered with an isotropic homogenous inner face layer made of metal and an isotropic homogenous outer one made of ceramic. The sandwich shell is modeled via Murakami's zig-zag theory, and the governing equations are derived using Hamilton's principle. An exact solution is presented for a simply supported shell via the Navier method to find the natural frequencies of the shell. The effects of various parameters on the natural frequencies are studied such as material gradation, the thickness-to-radius ratio, the core-to-face layers thickness ratio, and geometric factors of the auxetic cells. It is found that for each vibrational mode, an optimal ratio can be found between the thickness of the FGAH core and the thickness of the shell which leads to the highest natural frequency.

Keywords: Free vibration; Rotating shell; Auxetic honeycomb structure; Functionally graded material.

1 INTRODUCTION

THE main aims of utilizing sandwich structures rather than single-layer ones are to achieve high stiffness-to-mass and strength-to-mass ratios [1, 2] or to attain a smart structure whose mechanical properties can be

*Corresponding author. Tel.: +987144351093.
E-mail address: h.amirabadi@iauabadeh.ac.ir (Hossein Amirabadi)

affected by an external factor [3-8]. Structures that benefit from low density and tunable elastic constants can be selected as good choices to be used as a core in a sandwich structure. Since the core is not subjected to intense bending loads, it does not necessarily need to be of high rigidity and strength. Honeycombs are fragile but low-density structures that can be utilized as a core to attain a sandwich structure with an excellent value of stiffness-to-weight ratio. Thus, honeycomb structures have been used in various engineering fields such as transportation, civil, mechanical, and aerospace engineering. A fair amount of work has been presented in recent years to investigate the mechanical behavior of three-layered sandwich structures with honeycomb cores. As the most well-known type of honeycomb structure, the hexagonal one has been extensively used in various engineering fields [9-11]. In a hexagonal honeycomb structure, the Poisson's ratios are always positive values. However, other kinds of honeycomb structures have been proposed in recent years whose Poisson's ratios are negative values which are called auxetic honeycomb (AH) structures.

A fair amount of work has been presented in recent years associated with the mechanical analysis of sandwich structures with AH cores. Qing Tian and Zhi Chun [12] examined the wave propagation characteristics of a sandwich rectangular plate with an AH core and isotropic homogenous face layers. They examined the effects of the geometric parameters of the AH core on the wave propagation characteristics of the plate. The free and forced vibration analyses of a doubly-curved sandwich panel with an AH core subjected to blast load were studied by Duc et al. [13]. They focused on the impacts of the geometric parameters of the AH core on the dynamic deflection and natural frequencies of the shell. The dynamic response of a sandwich cylindrical shell with an AH core subjected to moving internal pressure was investigated by Eipakchi and Naserkani [14]. The effects of the geometric parameters of the AH core on the critical values of the frequency and velocity of the moving pressure were examined by them. The dynamic buckling and free vibration analyses of sandwich rectangular plates with an AH core and polymeric face sheets reinforced with graphene nanoplatelets (GNP) were studied by Nguyen et al. [15]. They studied the dependency of the natural frequencies and the stability regions on the geometric factors of the AH core. Xiao et al. [16] inspected the mechanical buckling analysis of a sandwich rectangular plate with an AH core and two laminated composite face sheets. They examined the effects of geometric factors of the AH core on the critical buckling load of the plate. Xu et al. [17] examined the free in-plane vibration behavior of an AH structure with curved sinusoidal walls. They focused on the optimization of such a structure and inspected the impacts of utilizing it on the energy absorption capacity of the structure and the amplitude of its oscillations. The free vibration analysis of a sandwich rectangular plate with an AH core and two FGM face sheets was studied by Pham et al. [18]. They focused on the effects of the geometric factors of the AH core on the natural frequencies of the plate. The nonlinear free and forced vibration analyses of an imperfect sandwich rectangular plate with an AH core and two piezoelectric face sheets were examined by Quan et al. [19]. They studied the dependency of the natural frequencies of the plate and the dynamic deflection on the geometric factors of the AH core.

Dat et al. [20] examined the nonlinear free and forced vibration analyses of a sandwich rectangular plate with an AH core and magneto-electro-elastic face sheets exposed to an explosive load. They inspected the influences of geometric factors of the AH core on the natural frequencies of the plate and the dynamic deflection. The thermal buckling and free vibration analyses of a viscoelastic doubly-curved sandwich shell with a tunable AH core and FGM face layers were examined by Li and Liu [21]. They focused on the effects of the geometric parameters of the AH core on the critical temperature and the natural frequencies of the shell. As a model of the wall of a fluid-filled tank, Pakrooyan et al. [22] investigated the free vibration analysis of a sandwich rectangular plate with an AH core and isotropic homogenous face sheets in contact with quiescent fluid. They studied the dependency of the natural frequencies on the geometric parameters of the AH core. Cong et al. [23] presented a parametric investigation to study the nonlinear free and forced vibration analyses of a doubly-curved sandwich panel with an AH core and two laminated polymeric face layers reinforced with carbon nanotubes (CNTs). They considered the temperature-dependency of the thermo-mechanical properties and examined the effect of geometric factors of the AH core on the natural frequencies and dynamic response of the shell. Liu et al. [24] studied the static bending analysis of a sandwich rectangular plate with a tunable AH core and FGM face sheets. The dependencies of the static deformation and stress distribution on the geometric parameters of the AH core were studied by them. The crashworthiness of hexachiral AH structures exposed to an in-plane loading was studied by Sadikbasha and Pandurangan [25]. They discussed the dependency of the energy absorption capacity of sandwich structures with hexachiral AH core on the geometric parameters of the cells. Necemer et al. [26] used the ANSYS software and analyzed the fatigue resistance of several AH structures. They compared five types of AH structures including re-entrant, S-shaped, star-shaped, chiral, and double arrowhead to check which one has the best fatigue resistance. Rai et al. [27] studied the dynamic response of a sandwich panel with an AH core subjected to explosive loading. They tried to optimize the energy absorption capacity of such a structure. Sarafraz et al. [28, 29] presented numerical solutions to analyze the mechanical buckling, the free vibration, and the flutter (aeroelastic stability) analyses of a sandwich rectangular

plate with an AH core and laminated three-phase polymer/GNP/fiber face sheets. They investigated the effects of the geometrical parameters of the AH core and the mass fraction of the fibers and GNPs on the critical buckling load, the natural frequencies, and the critical aerodynamic pressure of the plate.

The concept of FGM was introduced in the 1980s by some materials scientists in Japan [30]. This type of non-homogenous material is usually produced by the composition of two different materials including a ceramic phase and a metal phase whose volume fractions vary continuously in one, two, or even three directions. The main advantage of FGMs is their high resistance against simultaneous thermal and mechanical loads. Therefore, these materials have been used in various engineering fields such as civil, aerospace, and mechanical engineering. As a new idea to achieve low mass and high endurance against thermo-mechanical loading, recently, some researchers have proposed to produce AH structures from FGMs. To the best knowledge of the authors, there are few numbers of papers associated with the influences of FGAH cores on the mechanical behavior of sandwich plates and shells [31-34]. For the first time, an analytical solution is presented on the free vibration analysis of a sandwich cylindrical shell with a re-entrant FGAH core and two homogenous face layers. The sandwich shell is modeled based on the zig-zag theory. Three patterns are considered to describe the variations of the volume fractions of the metal and ceramic including power-law, sigmoid, and exponential functions. The effects of various factors on the natural frequencies of the shell are investigated including material gradation, the thickness-to-radius ratio, the core-to-face layers thickness ratio, and geometric factors of the auxetic cells. The results of this work can be useful in the design, analysis, and optimization of future aerospace structures.

2 MATHEMATICAL MODELING

2.1. Material Properties

As shown in Fig. 1, a three-layered sandwich cylindrical shell of mean radius R, length L, and total thickness h is considered. The sandwich shell consists of a re-entrant FGAH core of thickness h_c and isotropic homogeneous face layers of the same thickness $h_1=h_3=h_f=0.5(h-h_c)$. The inner and outer layers of the shell are fabricated from metal and ceramic, respectively.

The material properties of the non-homogeneous material utilized to fabricate the AH core vary from a metal-rich surface at the inner side of the core to a ceramic-rich one at the outer surface of the core according to a power-law function as [33]

$$\begin{aligned}
&\text{P-FGM:} \quad P_s(z)=P_m+(P_c-P_m)\left(\frac{1}{2}+\frac{z}{h_c}\right)^p,\\
&\text{S-FGM:} \quad P_s(z)=\begin{cases} P_m+0.5(P_c-P_m)\left(1+\dfrac{2z}{h_c}\right)^p, & -\dfrac{h_c}{2}\le z\le 0,\\ P_c-0.5(P_c-P_m)\left(1-\dfrac{2z}{h_c}\right)^p, & 0\le z\le \dfrac{h_c}{2}, \end{cases}\\
&\text{E-FGM:} \quad P_s(z)=P_m\exp\left[Ln\left(\frac{P_c}{P_m}\right)\left(\frac{1}{2}+\frac{z}{h_c}\right)^p\right],
\end{aligned} \tag{1}$$

where P stands for either the density (ρ_s), the elastic modulus (E_s), or the Poisson's ratio (ν_s), and the subscripts m and c indicate the material properties of the metal and ceramic phases, respectively. In Eq. (1), the dimensionless parameter p is called the material index which determines how the volume fractions of metal and ceramic vary in the thickness direction.

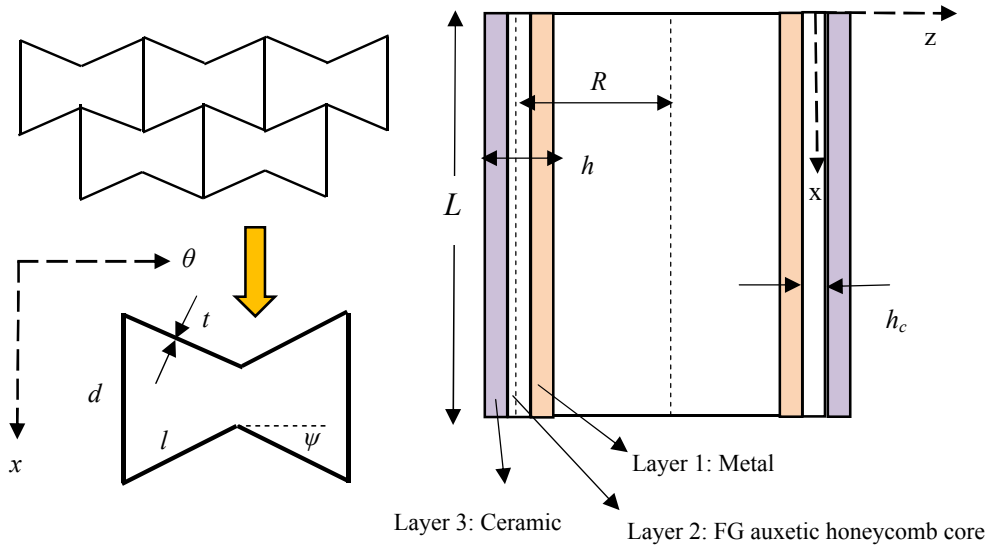

Fig. 1
A sandwich cylindrical shell with an FGAH core and isotropic homogeneous face layers.

The variations of material properties of the non-homogeneous material utilized to fabricate the AH core through the thickness direction are depicted in Fig. 2 for P_c/P_m=2 and several various values of the material index.

Since an FGM is an isotropic material, the shear modulus (G_s) of the material used to produce the AH core can be calculated through the relation below:

$$G_s = \frac{E_s}{2(1+\nu_s)}. \tag{2}$$

Referring to the geometric parameters of an individual cell of a re-entrant FGAH structure illustrated in Fig. 1, the elastic constants and the density of the FGAH core can be attained using the following relation [35]:

$$\frac{E_{xx}^{(2)}}{E_s} = \frac{\sec^3\psi\left(e_1-\sin\psi\right)e_2^3}{1+e_2^2\left(\tan^2\psi+e_1\sec^2\psi\right)}, \quad \frac{E_{\theta\theta}^{(2)}}{E_s} = \frac{e_2^3\sec\psi}{\left(e_1-\sin\psi\right)\left(\tan^2\psi+e_2^2\right)},$$
$$\frac{G_{\theta z}^{(2)}}{G_s} = \frac{e_2\cos\psi}{e_1-\sin\psi}, \quad \frac{G_{xz}^{(2)}}{G_s} = \frac{e_2\sec\psi}{2}\left[\frac{e_1-\sin\psi}{1+2e_1}+\frac{e_1+2\sin^2\psi}{2\left(e_1-\sin\psi\right)}\right], \quad \frac{G_{x\theta}^{(2)}}{E_s} = \frac{e_2^3\sec\psi}{e_1\left(1+2e_1\right)}, \tag{3}$$

$$\nu_{\theta x}^{(2)} = \frac{E_{\theta\theta}^{(2)}}{E_{xx}^{(2)}}\nu_{x\theta}^{(2)}, \quad \nu_{x\theta}^{(2)} = \frac{-\left(1-e_2^2\right)\left(e_1-\sin\psi\right)\sin\psi\sec^2\psi}{1+e_2^2\left(\tan^2\psi+e_1\sec^2\psi\right)}, \quad \frac{\rho^{(2)}}{\rho_s} = \frac{e_2\left(1+0.5e_1\right)\sec\psi}{e_1-\sin\psi},$$

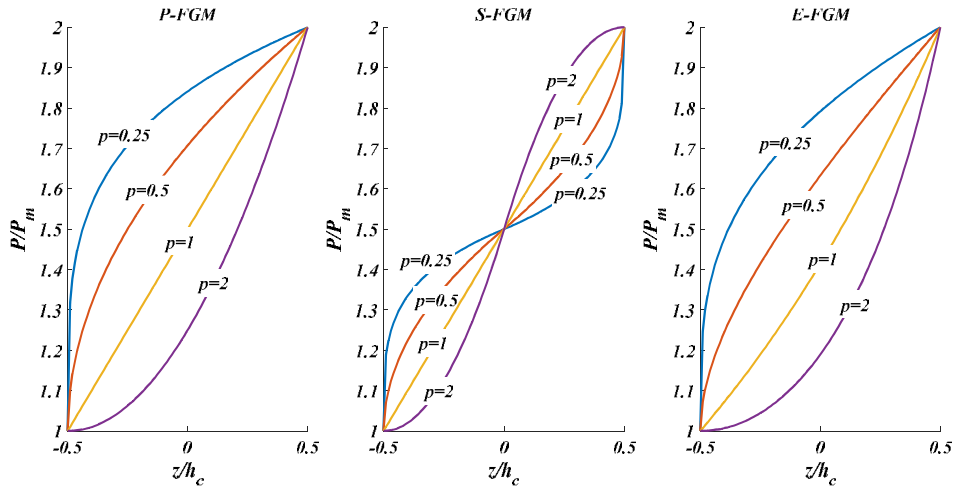

Fig. 2
Variations of material properties of the material utilized to fabricate the AH core through the thickness direction.

where

$$e_1 = \frac{d}{l}, \quad e_2 = \frac{t}{l}. \tag{4}$$

Eq. (3) indicates that the FGAH core is an orthotropic non-homogenous structure fabricated from an isotropic non-homogenous material.

The density and the elastic constants of the isotropic homogeneous inner and outer face layers can be presented as follows:

$$\begin{aligned} &\rho^{(1)} = \rho_m, \quad E^{(1)} = E_m, \quad \nu^{(1)} = \nu_m, \quad G^{(1)} = G_m = \frac{E_m}{2(1+\nu_m)}, \\ &\rho^{(3)} = \rho_c, \quad E^{(3)} = E_c, \quad \nu^{(3)} = \nu_c, \quad G^{(3)} = G_c = \frac{E_c}{2(1+\nu_c)}, \end{aligned} \tag{5}$$

where G_m and G_c are the shear moduli of the metal and ceramic phases, respectively.

2.2. Deformation, Strain, and Stress

Based on Murakami's zig-zag theory, the deformation field can be described as follows [36]:

$$\begin{aligned} u_1(t,z,x,\theta) &= u(t,x,\theta) + z\varphi_x(t,x,\theta) + f(z)s_x(x,\theta,t), \\ u_2(t,z,x,\theta) &= v(t,x,\theta) + z\varphi_\theta(t,x,\theta) + f(z)s_\theta(x,\theta,t), \\ u_3(t,z,x,\theta) &= w(t,x,\theta), \end{aligned} \tag{6}$$

where u_1, u_2, and u_3 show displacement along x, θ, and z directions, respectively, and φ_x and φ_θ are the rotations about θ and x axes, respectively. The variables s_x and s_θ are used to incorporate the zig-zag effect, and $f(z)$ is defined as follows [36]:

$$f(z) = \sum_{k=1}^{N_L} \frac{2(-1)^k}{h_k} \left[z - 0.5(z_k + z_{k+1}) \right] \left[H(z - z_k) - H(z - z_{k+1}) \right]. \tag{7}$$

where h_k represents the thickness of the kth layer, z_k and z_{k+1} are the transverse position of the bottom and top of the kth face layer, respectively, N_L stands for the number of layers which is 3 in this paper, and H is the well-known Heaviside function.

It is noteworthy that by removing s_x, s_θ, and $f(z)$ the well-known first-order shear deformation theory (FSDT) is attained. A schematical comparison between the displacement fields in the zig-zag and the FSDT theories is depicted in Fig. 3.

The normal (ε_{ij}) and shear ($\gamma_{ij}=2\varepsilon_{ij}$) components of the strain tensor can be calculated through the following relations [37, 38]:

$$\begin{aligned}
&\varepsilon_{xx}=\frac{\partial u_1}{\partial x}=\frac{\partial u}{\partial x}+z\frac{\partial \varphi_x}{\partial x}+f\frac{\partial s_x}{\partial x},\quad \varepsilon_{\theta\theta}=\frac{1}{R}\left(\frac{\partial u_2}{\partial \theta}+u_3\right)=\frac{1}{R}\left(\frac{\partial v}{\partial \theta}+z\frac{\partial \varphi_\theta}{\partial \theta}+f\frac{\partial s_\theta}{\partial \theta}+w\right),\\
&\varepsilon_{zz}=\frac{\partial u_3}{\partial z}=0,\quad \gamma_{x\theta}=\frac{1}{R}\frac{\partial u_1}{\partial \theta}+\frac{\partial u_2}{\partial x}=\frac{1}{R}\frac{\partial u}{\partial \theta}+\frac{\partial v}{\partial x}+z\left(\frac{1}{R}\frac{\partial \varphi_x}{\partial \theta}+\frac{\partial \varphi_\theta}{\partial x}\right)+f\left(\frac{1}{R}\frac{\partial s_x}{\partial \theta}+\frac{\partial s_\theta}{\partial x}\right),\\
&\gamma_{xz}=\frac{\partial u_1}{\partial z}+\frac{\partial u_3}{\partial x}=\varphi_x+\frac{\partial w}{\partial x}+g\,s_x,\quad \gamma_{\theta z}=\frac{\partial u_2}{\partial z}-\frac{u_2}{R}+\frac{1}{R}\frac{\partial u_3}{\partial \theta}=\varphi_\theta-\frac{v}{R}+\frac{1}{R}\frac{\partial w}{\partial \theta}+g\,s_\theta.
\end{aligned}\tag{8}$$

where

$$g(z)=\frac{df(z)}{dz}=\sum_{k=1}^{N_L}\frac{2(-1)^k}{h_k}\left[H(z-z_k)-H(z-z_{k+1})\right].\tag{9}$$

It should be noted that Eq. (7) is attained by considering the assumption of shallow shells:

$$1\pm\frac{z}{R}\approx 1,\quad 1\pm\frac{f}{Rg}\approx 1.\tag{10}$$

The non-zero components of the stress tensor (σ_{ij}) in the kth layer of the shell can be calculated as [39, 40]

$$\begin{Bmatrix}\sigma_{xx}^{(i)}\\ \sigma_{\theta\theta}^{(i)}\\ \sigma_{\theta z}^{(i)}\\ \sigma_{xz}^{(i)}\\ \sigma_{x\theta}^{(i)}\end{Bmatrix}=\begin{bmatrix}Q_{11}^{(i)} & Q_{12}^{(i)} & 0 & 0 & 0\\ Q_{12}^{(i)} & Q_{22}^{(i)} & 0 & 0 & 0\\ 0 & 0 & k_sQ_{44}^{(i)} & 0 & 0\\ 0 & 0 & 0 & k_sQ_{55}^{(i)} & 0\\ 0 & 0 & 0 & 0 & Q_{66}^{(i)}\end{bmatrix}\begin{Bmatrix}\varepsilon_{xx}\\ \varepsilon_{\theta\theta}\\ \gamma_{\theta z}\\ \gamma_{xz}\\ \gamma_{x\theta}\end{Bmatrix},\tag{11}$$

where k_s=5/6 is the well-known shear correction factor and

$$Q_{11}^{(i)}=\frac{E_{xx}^{(i)}}{1-\nu_{\theta x}^{(i)}\nu_{x\theta}^{(i)}},\quad Q_{22}^{(i)}=\frac{E_{\theta\theta}^{(i)}}{1-\nu_{\theta x}^{(i)}\nu_{x\theta}^{(i)}},\quad Q_{12}^{(i)}=\nu_{x\theta}^{(i)}Q_{\theta\theta}^{(i)},\quad Q_{44}^{(i)}=G_{\theta z}^{(i)},\quad Q_{55}^{(i)}=G_{xz}^{(i)},\quad Q_{66}^{(i)}=G_{x\theta}^{(i)}.\tag{12}$$

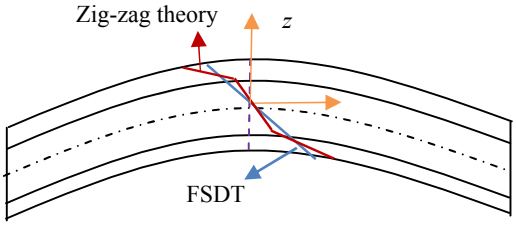

Fig. 3

The deformation in the zig-zag and the FSDT theories.

2.3. Hamilton's Principle

According to Hamilton's principle, the governing equations and boundary conditions regarding the vibration analysis of a structure can be obtained using the relation below [41, 42]:

$$\int_{t_1}^{t_2}\left(-\delta U+\delta T+\delta W_{n.c.}\right)dt=0, \tag{13}$$

in which δ is the well-known variational operator, t shows time, $[t_1,t_2]$ represents an arbitrary time interval, and. U, T, and $W_{n.c.}$ indicate the strain energy of the shell, the kinetic energy of the shell, and the work done by non-conservative external loads, respectively.

The variation of the strain energy of the shell can be described as follows [41]:

$$\delta U=\iiint_V\left(\sigma_{xx}\delta\varepsilon_{xx}+\sigma_{\theta\theta}\delta\varepsilon_{\theta\theta}+\sigma_{x\theta}\delta\gamma_{x\theta}+\sigma_{xz}\delta\gamma_{xz}+\sigma_{\theta z}\delta\gamma_{\theta z}\right)dV, \tag{14}$$

in which V shows the volume of the shell and is defined as

$$\iiint_V(\ )dV=\iint_S\int_{-\frac{h}{2}}^{\frac{h}{2}}(\ )dzdS, \tag{15}$$

where $dS=Rdxd\theta$ is the surface of the shell at the middle surface (z=0).

Utilizing Eqs. (8), (14), and (15), the following relation can be presented:

$$\begin{aligned}\delta U=\iint_S\Bigg[&N_{xx}\frac{\partial\delta u}{\partial x}+M_{xx}\frac{\partial\delta\varphi_x}{\partial x}+P_{xx}\frac{\partial\delta s_x}{\partial x}+\frac{N_{\theta\theta}}{R}\left(\frac{\partial\delta v}{\partial\theta}+\delta w\right)+\frac{M_{\theta\theta}}{R}\frac{\partial\delta\varphi_\theta}{\partial\theta}+\frac{P_{\theta\theta}}{R}\frac{\partial\delta s_\theta}{\partial\theta}\\&+N_{x\theta}\left(\frac{1}{R}\frac{\partial\delta u}{\partial\theta}+\frac{\partial\delta v}{\partial x}\right)M_{x\theta}+\left(\frac{1}{R}\frac{\partial\delta\varphi_x}{\partial\theta}+\frac{\partial\delta\varphi_\theta}{\partial x}\right)+P_{x\theta}\left(\frac{1}{R}\frac{\partial\delta s_x}{\partial\theta}+\frac{\partial\delta s_\theta}{\partial x}\right)\\&+Q_{xz}\left(\frac{\partial\delta w}{\partial x}+\delta\varphi_x\right)+R_{xz}\delta s_x+Q_{\theta z}\left(-\frac{\delta v}{R}+\frac{1}{R}\frac{\partial\delta w}{\partial\theta}+\delta\varphi_\theta\right)+R_{\theta z}\delta s_\theta\Bigg]dS.\end{aligned} \tag{16}$$

where

$$\begin{Bmatrix}N_{ij}\\M_{ij}\\P_{ij}\end{Bmatrix}=\int_{-\frac{h}{2}}^{\frac{h}{2}}\sigma_{ij}\begin{Bmatrix}1\\z\\f(z)\end{Bmatrix}dz,\quad\begin{Bmatrix}Q_{iz}\\R_{iz}\end{Bmatrix}=\int_{-\frac{h}{2}}^{\frac{h}{2}}\sigma_{iz}\begin{Bmatrix}1\\g(z)\end{Bmatrix}dz,\quad i,j=x,\theta. \tag{17}$$

By substituting Eqs. (8) and (11) into Eq. (17), one can write the relation below:

$$\begin{Bmatrix}N_{xx}\\N_{\theta\theta}\\M_{xx}\\M_{\theta\theta}\\P_{xx}\\P_{\theta\theta}\end{Bmatrix}=\begin{bmatrix}A_{11}&A_{12}&B_{11}&B_{12}&F_{11}&F_{12}\\A_{12}&A_{22}&B_{12}&B_{22}&F_{12}&F_{22}\\B_{11}&B_{12}&D_{11}&D_{12}&H_{11}&H_{12}\\B_{12}&B_{22}&D_{12}&D_{22}&H_{12}&H_{22}\\F_{11}&F_{12}&H_{11}&H_{12}&T_{11}&T_{12}\\F_{12}&F_{22}&H_{12}&H_{22}&T_{12}&T_{22}\end{bmatrix}\begin{Bmatrix}\frac{\partial u}{\partial x}\\\frac{1}{R}\left(\frac{\partial v}{\partial\theta}+w\right)\\\frac{\partial\varphi_x}{\partial x}\\\frac{1}{R}\frac{\partial\varphi_\theta}{\partial\theta}\\\frac{\partial s_x}{\partial x}\\\frac{1}{R}\frac{\partial s_\theta}{\partial\theta}\end{Bmatrix},\quad\begin{Bmatrix}N_{x\theta}\\M_{x\theta}\\P_{x\theta}\end{Bmatrix}=\begin{bmatrix}A_{66}&B_{66}&F_{66}\\B_{66}&D_{66}&H_{66}\\F_{66}&H_{66}&T_{66}\end{bmatrix}\begin{Bmatrix}\frac{1}{R}\frac{\partial u}{\partial\theta}+\frac{\partial v}{\partial x}\\\frac{1}{R}\frac{\partial\varphi_x}{\partial\theta}+\frac{\partial\varphi_\theta}{\partial x}\\\frac{1}{R}\frac{\partial s_x}{\partial\theta}+\frac{\partial s_\theta}{\partial x}\end{Bmatrix}, \tag{18}$$

$$\begin{Bmatrix}Q_{\theta z}\\R_{\theta z}\end{Bmatrix}=\begin{bmatrix}A_{44}&Y_{44}\\Y_{44}&Z_{44}\end{bmatrix}\begin{Bmatrix}-\frac{v}{R}+\frac{1}{R}\frac{\partial w}{\partial\theta}+\varphi_\theta\\s_\theta\end{Bmatrix},\quad\begin{Bmatrix}Q_{xz}\\R_{xz}\end{Bmatrix}=\begin{bmatrix}A_{55}&Y_{55}\\Y_{55}&Z_{55}\end{bmatrix}\begin{Bmatrix}\frac{\partial w}{\partial x}+\varphi_x\\s_x\end{Bmatrix},$$

in which the stiffness coefficients are defined as follows:

$$\begin{Bmatrix} A_{ij} \\ B_{ij} \\ D_{ij} \\ F_{ij} \\ H_{ij} \\ T_{ij} \end{Bmatrix} = \int_{-\frac{h}{2}}^{\frac{h}{2}} Q_{ij}(z) \begin{Bmatrix} 1 \\ z \\ z^2 \\ f(z) \\ zf(z) \\ f^2(z) \end{Bmatrix} dz, \quad \begin{Bmatrix} A_{kk} \\ Y_{kk} \\ Z_{kk} \end{Bmatrix} = k_s \int_{-\frac{h}{2}}^{\frac{h}{2}} Q_{kk}(z) \begin{Bmatrix} 1 \\ g(z) \\ g^2(z) \end{Bmatrix} dz, \quad \begin{matrix} i,j = 1,2,6. \\ k = 4,5. \end{matrix} \tag{19}$$

The equation below describes the variation of the kinetic energy of the shell [41]:

$$\delta T = \iiint_V \rho \left(\frac{\partial \delta u_1}{\partial t} \frac{\partial u_1}{\partial t} + \frac{\partial \delta u_2}{\partial t} \frac{\partial u_2}{\partial t} + \frac{\partial \delta u_3}{\partial t} \frac{\partial u_3}{\partial t} \right) dV, \tag{20}$$

Utilizing Eqs. (6) and (15), Eq. (20) can be represented as follows:

$$\begin{aligned} \delta T = \iint_S \Bigg[& J_0 \left(\frac{\partial u}{\partial t} \frac{\partial \delta u}{\partial t} + \frac{\partial v}{\partial t} \frac{\partial \delta v}{\partial t} + \frac{\partial w}{\partial t} \frac{\partial \delta w}{\partial t} \right) + J_1 \left(\frac{\partial \varphi_x}{\partial t} \frac{\partial \delta u}{\partial t} + \frac{\partial u}{\partial t} \frac{\partial \delta \varphi_x}{\partial t} + \frac{\partial \varphi_\theta}{\partial t} \frac{\partial \delta v}{\partial t} + \frac{\partial v}{\partial t} \frac{\partial \delta \varphi_\theta}{\partial t} \right) \\ & + J_2 \left(\frac{\partial \varphi_x}{\partial t} \frac{\partial \delta \varphi_x}{\partial t} + \frac{\partial \varphi_\theta}{\partial t} \frac{\partial \delta \varphi_\theta}{\partial t} \right) + J_3 \left(\frac{\partial s_x}{\partial t} \frac{\partial \delta u}{\partial t} + \frac{\partial u}{\partial t} \frac{\partial \delta s_x}{\partial t} + \frac{\partial s_\theta}{\partial t} \frac{\partial \delta v}{\partial t} + \frac{\partial v}{\partial t} \frac{\partial \delta s_\theta}{\partial t} \right) \\ & + J_4 \left(\frac{\partial s_x}{\partial t} \frac{\partial \delta \varphi_x}{\partial t} + \frac{\partial \varphi_x}{\partial t} \frac{\partial \delta s_x}{\partial t} + \frac{\partial s_\theta}{\partial t} \frac{\partial \delta \varphi_\theta}{\partial t} + \frac{\partial \varphi_\theta}{\partial t} \frac{\partial \delta s_\theta}{\partial t} \right) + J_5 \left(\frac{\partial s_x}{\partial t} \frac{\partial \delta s_x}{\partial t} + \frac{\partial s_\theta}{\partial t} \frac{\partial \delta s_\theta}{\partial t} \right) \Bigg] dS. \end{aligned} \tag{21}$$

where

$$\begin{Bmatrix} J_0 \\ J_1 \\ J_2 \\ J_3 \\ J_4 \\ J_5 \end{Bmatrix} = \int_{-\frac{h}{2}}^{\frac{h}{2}} \rho(z) \begin{Bmatrix} 1 \\ z \\ z^2 \\ f(z) \\ zf(z) \\ f^2(z) \end{Bmatrix} dz. \tag{22}$$

Substituting Eqs. (16) and (21) into Eq. (13) and considering $W_{n.c.}$=0 for the free vibration analysis, the following relations can be attained as the governing equations:

$$\begin{aligned} & J_0 \frac{\partial^2 u}{\partial t^2} + J_1 \frac{\partial^2 \varphi_x}{\partial t^2} + J_3 \frac{\partial^2 s_x}{\partial t^2} - \frac{\partial N_{xx}}{\partial x} - \frac{1}{R} \frac{\partial N_{x\theta}}{\partial \theta} = 0, \\ & J_0 \frac{\partial^2 v}{\partial t^2} + J_1 \frac{\partial^2 \varphi_\theta}{\partial t^2} + J_3 \frac{\partial^2 \varphi_\theta}{\partial t^2} - \frac{\partial N_{x\theta}}{\partial x} - \frac{1}{R} \frac{\partial N_{\theta\theta}}{\partial \theta} - \frac{Q_{\theta z}}{R} = 0, \\ & J_0 \frac{\partial^2 w}{\partial t^2} - \frac{\partial Q_{xz}}{\partial x} - \frac{1}{R} \frac{\partial Q_{\theta z}}{\partial \theta} + \frac{N_{\theta\theta}}{R} = 0, \\ & J_1 \frac{\partial^2 u}{\partial t^2} + J_2 \frac{\partial^2 \varphi_x}{\partial t^2} + J_4 \frac{\partial^2 s_x}{\partial t^2} - \frac{\partial M_{xx}}{\partial x} - \frac{1}{R} \frac{\partial M_{x\theta}}{\partial \theta} + Q_{xz} = 0, \\ & J_1 \frac{\partial^2 v}{\partial t^2} + J_2 \frac{\partial^2 \varphi_\theta}{\partial t^2} + J_4 \frac{\partial^2 s_\theta}{\partial t^2} - \frac{\partial M_{x\theta}}{\partial x} - \frac{1}{R} \frac{\partial M_{\theta\theta}}{\partial \theta} + Q_{\theta z} = 0, \\ & J_3 \frac{\partial^2 u}{\partial t^2} + J_4 \frac{\partial^2 \varphi_x}{\partial t^2} + J_5 \frac{\partial^2 s_x}{\partial t^2} - \frac{\partial P_{xx}}{\partial x} - \frac{1}{R} \frac{\partial P_{x\theta}}{\partial \theta} + R_{xz} = 0, \\ & J_3 \frac{\partial^2 v}{\partial t^2} + J_4 \frac{\partial^2 \varphi_\theta}{\partial t^2} + J_5 \frac{\partial^2 s_\theta}{\partial t^2} - \frac{\partial P_{x\theta}}{\partial x} - \frac{1}{R} \frac{\partial P_{\theta\theta}}{\partial \theta} + R_{\theta z} = 0. \end{aligned} \tag{23}$$

Also, the following equations describe the boundary conditions for simply supported edges at x=0 & L:

$$N_{xx} = 0, \quad v = 0, \quad w = 0, \quad M_{xx} = 0, \quad \varphi_\theta = 0, \quad P_{xx} = 0, \quad s_\theta = 0. \tag{24}$$

Substituting Eq. (18) into Eq. (24) leads to the relations below as the governing equations:

$$
\begin{aligned}
&-A_{11}\frac{\partial^2 u}{\partial x^2}-\frac{A_{66}}{R^2}\frac{\partial^2 u}{\partial \theta^2}-\frac{A_{12}+A_{66}}{R}\frac{\partial^2 v}{\partial x\partial \theta}-\frac{A_{12}}{R}\frac{\partial w}{\partial x}-B_{11}\frac{\partial^2 \varphi_x}{\partial x^2}-\frac{B_{66}}{R^2}\frac{\partial^2 \varphi_x}{\partial \theta^2}-\frac{B_{12}+B_{66}}{R}\frac{\partial^2 \varphi_\theta}{\partial x\partial \theta}\\
&-F_{11}\frac{\partial^2 s_x}{\partial x^2}-\frac{F_{66}}{R^2}\frac{\partial^2 s_x}{\partial \theta^2}-\frac{F_{12}+F_{66}}{R}\frac{\partial^2 s_\theta}{\partial x\partial \theta}=-J_0\frac{\partial^2 u}{\partial t^2}-J_1\frac{\partial^2 \varphi_x}{\partial t^2}-J_3\frac{\partial^2 s_x}{\partial t^2},
\end{aligned}
$$

$$
\begin{aligned}
&-\frac{A_{12}+A_{66}}{R}\frac{\partial^2 u}{\partial x\partial \theta}-A_{66}\frac{\partial^2 v}{\partial x^2}-\frac{A_{22}}{R^2}\frac{\partial^2 v}{\partial \theta^2}+\frac{A_{44}}{R^2}v-\frac{A_{22}+A_{44}}{R^2}\frac{\partial w}{\partial \theta}-\frac{B_{12}+B_{66}}{R}\frac{\partial^2 \varphi_x}{\partial x\partial \theta}-B_{66}\frac{\partial^2 \varphi_\theta}{\partial x^2}\\
&-\frac{B_{22}}{R^2}\frac{\partial^2 \varphi_\theta}{\partial \theta^2}-\frac{A_{44}}{R}\varphi_\theta-\frac{F_{12}+F_{66}}{R}\frac{\partial^2 s_x}{\partial x\partial \theta}-F_{66}\frac{\partial^2 s_\theta}{\partial x^2}-\frac{F_{22}}{R^2}\frac{\partial^2 s_\theta}{\partial \theta^2}-\frac{Y_{44}}{R}s_\theta=-J_0\frac{\partial^2 v}{\partial t^2}-J_1\frac{\partial^2 \varphi_\theta}{\partial t^2}-J_3\frac{\partial^2 \varphi_\theta}{\partial t^2},
\end{aligned}
$$

$$
\begin{aligned}
&\frac{A_{12}}{R}\frac{\partial u}{\partial x}+\frac{A_{22}+A_{44}}{R^2}\frac{\partial v}{\partial \theta}-A_{55}\frac{\partial^2 w}{\partial x^2}-\frac{A_{44}}{R^2}\frac{\partial^2 w}{\partial \theta^2}+\frac{A_{22}}{R^2}w-\left(A_{55}-\frac{B_{12}}{R}\right)\frac{\partial \varphi_x}{\partial x}\\
&-\frac{1}{R}\left(A_{44}-\frac{B_{22}}{R}\right)\frac{\partial \varphi_\theta}{\partial \theta}-\left(Y_{55}-\frac{F_{12}}{R}\right)\frac{\partial s_x}{\partial x}-\frac{1}{R}\left(Y_{44}-\frac{F_{22}}{R}\right)\frac{\partial s_\theta}{\partial \theta}=-J_0\frac{\partial^2 w}{\partial t^2},
\end{aligned}
$$

$$
\begin{aligned}
&-B_{11}\frac{\partial^2 u}{\partial x^2}-\frac{B_{66}}{R^2}\frac{\partial^2 u}{\partial \theta^2}-\frac{B_{12}+B_{66}}{R}\frac{\partial^2 v}{\partial x\partial \theta}+\left(A_{55}-\frac{B_{12}}{R}\right)\frac{\partial w}{\partial x}-D_{11}\frac{\partial^2 \varphi_x}{\partial x^2}-\frac{D_{66}}{R^2}\frac{\partial^2 \varphi_x}{\partial \theta^2}+A_{55}\varphi_x\\
&-\frac{D_{12}+D_{66}}{R}\frac{\partial^2 \varphi_\theta}{\partial x\partial \theta}-H_{11}\frac{\partial^2 s_x}{\partial x^2}-\frac{H_{66}}{R^2}\frac{\partial^2 s_x}{\partial \theta^2}+Y_{55}s_x-\frac{H_{12}+H_{66}}{R}\frac{\partial^2 s_\theta}{\partial x\partial \theta}=-J_1\frac{\partial^2 u}{\partial t^2}-J_2\frac{\partial^2 \varphi_x}{\partial t^2}-J_4\frac{\partial^2 s_x}{\partial t^2},
\end{aligned}
\tag{25}
$$

$$
\begin{aligned}
&-\frac{B_{12}+B_{66}}{R}\frac{\partial^2 u}{\partial x\partial \theta}-B_{66}\frac{\partial^2 v}{\partial x^2}-\frac{B_{22}}{R^2}\frac{\partial^2 v}{\partial \theta^2}-\frac{A_{44}}{R}v+\frac{1}{R}\left(A_{44}-\frac{B_{22}}{R}\right)\frac{\partial w}{\partial \theta}-\frac{D_{12}+D_{66}}{R}\frac{\partial^2 \varphi_x}{\partial x\partial \theta}-D_{66}\frac{\partial^2 \varphi_\theta}{\partial x^2}\\
&-\frac{D_{22}}{R^2}\frac{\partial^2 \varphi_\theta}{\partial \theta^2}+A_{44}\varphi_\theta-\frac{H_{12}+H_{66}}{R}\frac{\partial^2 s_x}{\partial x\partial \theta}-H_{66}\frac{\partial^2 s_\theta}{\partial x^2}-\frac{H_{22}}{R^2}\frac{\partial^2 s_\theta}{\partial \theta^2}+Y_{44}s_\theta=-J_1\frac{\partial^2 v}{\partial t^2}-J_2\frac{\partial^2 \varphi_\theta}{\partial t^2}-J_4\frac{\partial^2 s_\theta}{\partial t^2},
\end{aligned}
$$

$$
\begin{aligned}
&-F_{11}\frac{\partial^2 u}{\partial x^2}-\frac{F_{66}}{R^2}\frac{\partial^2 u}{\partial \theta^2}-\frac{F_{12}+F_{66}}{R}\frac{\partial^2 v}{\partial x\partial \theta}+\left(Y_{55}-\frac{F_{12}}{R}\right)\frac{\partial w}{\partial x}-H_{11}\frac{\partial^2 \varphi_x}{\partial x^2}-\frac{H_{66}}{R^2}\frac{\partial^2 \varphi_x}{\partial \theta^2}+Y_{55}\varphi_x\\
&-\frac{H_{12}+H_{66}}{R}\frac{\partial^2 \varphi_\theta}{\partial x\partial \theta}-T_{11}\frac{\partial^2 s_x}{\partial x^2}-\frac{T_{66}}{R^2}\frac{\partial^2 s_x}{\partial \theta^2}+Z_{55}s_x-\frac{T_{12}+T_{66}}{R}\frac{\partial^2 s_\theta}{\partial x\partial \theta}=-J_3\frac{\partial^2 u}{\partial t^2}-J_4\frac{\partial^2 \varphi_x}{\partial t^2}-J_5\frac{\partial^2 s_x}{\partial t^2},
\end{aligned}
$$

$$
\begin{aligned}
&-\frac{F_{12}+F_{66}}{R}\frac{\partial^2 u}{\partial x\partial \theta}-F_{66}\frac{\partial^2 v}{\partial x^2}-\frac{F_{22}}{R^2}\frac{\partial^2 v}{\partial \theta^2}-\frac{Y_{44}}{R}v+\frac{1}{R}\left(Y_{44}-\frac{F_{22}}{R}\right)\frac{\partial w}{\partial \theta}-\frac{H_{12}+H_{66}}{R}\frac{\partial^2 \varphi_x}{\partial x\partial \theta}-H_{66}\frac{\partial^2 \varphi_\theta}{\partial x^2}\\
&-\frac{H_{22}}{R^2}\frac{\partial^2 \varphi_\theta}{\partial \theta^2}+Y_{44}\varphi_\theta-\frac{T_{12}+T_{66}}{R}\frac{\partial^2 s_x}{\partial x\partial \theta}-T_{66}\frac{\partial^2 s_\theta}{\partial x^2}-\frac{T_{22}}{R^2}\frac{\partial^2 s_\theta}{\partial \theta^2}+Z_{44}s_\theta=-J_3\frac{\partial^2 v}{\partial t^2}-J_4\frac{\partial^2 \varphi_\theta}{\partial t^2}-J_5\frac{\partial^2 s_\theta}{\partial t^2}.
\end{aligned}
$$

Substituting Eq. (18) into Eq. (21) provides the following equations as the boundary conditions:

$$
\begin{aligned}
&A_{11}\frac{\partial u}{\partial x}+\frac{A_{12}}{R}\left(\frac{\partial v}{\partial \theta}+w\right)+B_{11}\frac{\partial \varphi_x}{\partial x}+\frac{B_{12}}{R}\frac{\partial \varphi_\theta}{\partial \theta}+F_{11}\frac{\partial s_x}{\partial x}+\frac{F_{12}}{R}\frac{\partial s_\theta}{\partial \theta}=0,\quad v=0,\quad w=0,\\
&B_{11}\frac{\partial u}{\partial x}+\frac{B_{12}}{R}\left(\frac{\partial v}{\partial \theta}+w\right)+D_{11}\frac{\partial \varphi_x}{\partial x}+\frac{D_{12}}{R}\frac{\partial \varphi_\theta}{\partial \theta}+H_{11}\frac{\partial s_x}{\partial x}+\frac{H_{12}}{R}\frac{\partial s_\theta}{\partial \theta}=0,\quad \varphi_\theta=0,\\
&F_{11}\frac{\partial u}{\partial x}+\frac{F_{12}}{R}\left(\frac{\partial v}{\partial \theta}+w\right)+H_{11}\frac{\partial \varphi_x}{\partial x}+\frac{H_{12}}{R}\frac{\partial \varphi_\theta}{\partial \theta}+T_{11}\frac{\partial s_x}{\partial x}+\frac{T_{12}}{R}\frac{\partial s_\theta}{\partial \theta}=0,\quad s_\theta=0,
\end{aligned}
\tag{26}
$$

which results in the following simplified form:

$$
\frac{\partial u}{\partial x}=0,\quad v=0,\quad w=0,\quad \frac{\partial \varphi_x}{\partial x}=0,\quad \varphi_\theta=0.\quad \frac{\partial s_x}{\partial x}=0,\quad s_\theta=0.
\tag{27}
$$

3 SOLUTION PROCEDURE

Utilizing the Navier solution, the relations below can be considered to satisfy the simply supported boundary conditions presented in Eq. (27) at both edges of the shell [43]:

$$\begin{Bmatrix} u(t,x,\theta) \\ v(t,x,\theta) \\ w(t,x,\theta) \\ \varphi_x(t,x,\theta) \\ \varphi_\theta(t,x,\theta) \\ s_x(t,x,\theta) \\ s_\theta(t,x,\theta) \end{Bmatrix} = \sum_{m=1}^{\infty}\sum_{n=0}^{\infty} \begin{Bmatrix} U_{mn}\cos(\alpha x)\cos(n\theta) \\ V_{mn}\sin(\alpha x)\sin(n\theta) \\ W_{mn}\sin(\alpha x)\cos(n\theta) \\ X_{mn}\cos(\alpha x)\cos(n\theta) \\ \Theta_{mn}\sin(\alpha x)\sin(n\theta) \\ Y_{mn}\cos(\alpha x)\cos(n\theta) \\ Z_{mn}\sin(\alpha x)\sin(n\theta) \end{Bmatrix} \exp(i\omega t), \quad \alpha = \frac{m\pi}{L}, \tag{28}$$

in which ω is the natural frequency, and m=1,2,3,… and n=0,1,2,… are known as the longitudinal and circumferential wave numbers, respectively.

Inserting Eq. (28) into Eq. (25) results in the following relation:

$$[K]\begin{Bmatrix} U_{mn} \\ V_{mn} \\ W_{mn} \\ X_{mn} \\ \Phi_{mn} \\ Y_{mn} \\ Z_{mn} \end{Bmatrix} = \omega^2 [M] \begin{Bmatrix} U_{mn} \\ V_{mn} \\ W_{mn} \\ X_{mn} \\ \Phi_{mn} \\ Y_{mn} \\ Z_{mn} \end{Bmatrix}, \tag{29}$$

where, as defined in Eq. (30), [K] and [M] are stiffness and mass matrixes, consecutively:

$$\begin{aligned}
&k_{11} = \alpha^2 A_{11} + \frac{A_{66}n^2}{R^2}, \quad k_{12} = -\frac{n\alpha(A_{12}+A_{66})}{R}, \quad k_{13} = -\frac{\alpha A_{12}}{R}, \quad k_{14} = \alpha^2 B_{11} + \frac{B_{66}n^2}{R^2}, \quad k_{15} = -\frac{n\alpha(B_{12}+B_{66})}{R}, \\
&k_{16} = \alpha^2 F_{11} + \frac{F_{66}n^2}{R^2}, \quad k_{17} = -\frac{n\alpha(F_{12}+F_{66})}{R}, \quad m_{11} = J_0, \quad m_{14} = J_1, \quad m_{16} = J_3, \quad m_{12} = m_{13} = m_{15} = m_{17} = 0, \\
&k_{22} = \alpha^2 A_{66} + \frac{A_{22}n^2 + A_{44}}{R^2}, \quad k_{23} = \frac{n(A_{22}+A_{44})}{R^2}, \quad k_{24} = -\frac{n\alpha(B_{12}+B_{66})}{R}, \quad k_{25} = \alpha^2 B_{66} + \frac{B_{22}n^2}{R^2} - \frac{A_{44}}{R}, \\
&k_{26} = -\frac{n\alpha(F_{12}+F_{66})}{R}, \quad k_{27} = \alpha^2 F_{66} + \frac{F_{22}n^2}{R^2} - \frac{Y_{44}}{R}, \quad m_{22} = J_0, \quad m_{25} = J_1, \quad m_{27} = J_3, \quad m_{23} = m_{24} = m_{26} = 0, \\
&k_{33} = \alpha^2 A_{55} + \frac{A_{22}+A_{44}n^2}{R^2}, \quad k_{34} = \alpha\left(A_{55} - \frac{B_{12}}{R}\right), \quad k_{35} = -\frac{n}{R}\left(A_{44} - \frac{B_{22}}{R}\right), \quad k_{36} = \alpha\left(Y_{55} - \frac{F_{12}}{R}\right), \\
&k_{37} = -\frac{n}{R}\left(Y_{44} - \frac{F_{22}}{R}\right), \quad m_{33} = J_0, \quad m_{34} = m_{35} = m_{36} = m_{37} = 0, \quad k_{44} = \alpha^2 D_{11} + \frac{D_{66}n^2}{R^2} + A_{55}, \\
&k_{45} = -\frac{n\alpha(D_{12}+D_{66})}{R}, \quad k_{46} = \alpha^2 H_{11} + \frac{H_{66}n^2}{R^2} + Y_{55}, \quad k_{47} = -\frac{n\alpha(H_{12}+H_{66})}{R}, \quad m_{44} = J_2, \\
&m_{46} = J_4, \quad m_{45} = m_{47} = 0, \quad k_{55} = \alpha^2 D_{66} + \frac{D_{22}n^2}{R^2} + A_{44}, \quad k_{56} = -\frac{n\alpha(H_{12}+H_{66})}{R}, \quad k_{57} = \alpha^2 H_{66} + \frac{H_{22}n^2}{R^2} + Y_{44}, \\
&m_{55} = J_2, \quad m_{56} = 0, \quad m_{57} = J_4, \quad k_{66} = \alpha^2 T_{11} + \frac{T_{66}n^2}{R^2} + Z_{55}, \quad k_{67} = -\frac{n\alpha(T_{12}+T_{66})}{R}, \quad m_{66} = J_5, \\
&m_{67} = 0, \quad k_{77} = \alpha^2 T_{66} + \frac{T_{22}n^2}{R^2} + Z_{44}, \quad m_{77} = J_5.
\end{aligned} \tag{30}$$

Through the solution of the eigenvalue Eq. (30), the natural frequencies of the shell can be attained. In the presented work, the dimensionless natural frequency is defined as follows:

$$\lambda_{nm} = \omega_{nm} R \sqrt{\frac{\rho_m}{E_m}}. \tag{31}$$

4 NUMERICAL EXAMPLES

4.1. Verification

To confirm the accuracy of the presented simulation, a single-layer P-FGM cylindrical shell of R=1 m, h/R=0.002, and L/R=20 is considered. The mechanical properties change from the mechanical properties of nickel (ρ_1=8900 kg/m^3, E_1=205.098 GPa, v_1=0.31) at the inner surface of the shell to the mechanical properties of stainless steel (ρ_2=8166 kg/m^3, E_2=207.788 GPa, v_2=0.317756) at its outer surface. For several values of the circumferential wave number and various values of the material index, the natural frequencies are reported in Table 1 m=1 against the corresponding ones reported by Loy et al. [44]. As observed, the results are in high agreement which proves the precision of the present work.

4.1. Parametric Study

In the current section, a parametric study is presented to examine the dependency of the natural frequencies on several factors such as material gradation, the core-to-face layers thickness ratio, and geometric parameters of the re-entrant cells. Except for the cases which are stated otherwise, numerical results are presented for a sandwich cylindrical shell of R=0.2 m, h/R=0.05, and L/R=5. Aluminum (Al) and Alumina (Al_2O_3) (ρ_m=2700 kg/m^3, E_m=70 GPa, v_m=0.35, ρ_c=3950 kg/m^3, E_c=380 GPa, v_c=0.22) are selected as metal and ceramic phases, respectively. The FGAH core is of type P-FGM with h_c/h=0.7, p=0.5, e_1=2, e_2=0.02, and ψ=30°. It is obvious that the face layers are of the same thickness h_1=h_3=0.15h. For some values of the axial wave number (m=1,2,3,4), the variations of the natural frequencies of the shell versus the variation of the circumferential wave number are depicted in Fig. 4. As observed, by increasing the circumferential wave number, the natural frequencies experience and initial reduction followed by a steadily increase. This figure shows that the first to fourth lowest natural frequencies belong to vibrational modes associated with (n,m)=(2,1), (n,m)=(3,1), (n,m)=(3,2), and (n,m)=(1,1), respectively. The dimensionless natural frequencies and the corresponding mode shapes are presented in Fig. 5. In what follows, the parametric study is presented to examine the effects of various parameters on the natural frequencies associated with these vibrational modes.

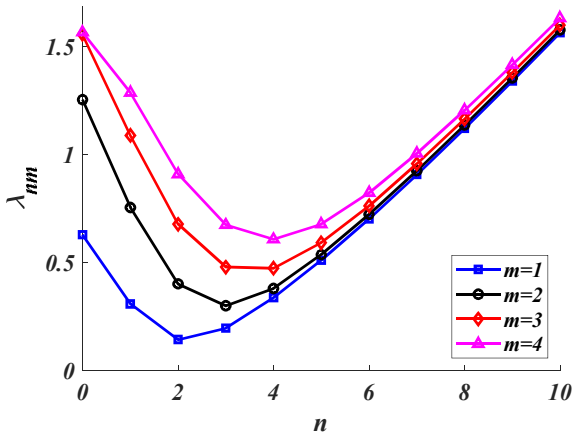

Fig. 4
The effects of circumferential and axial wave numbers on the natural frequencies of the shell.

Table 1
The natural frequencies of a single layer FGM cylindrical shell in Hz (R=1 m, h/R=0.002, L/R=20, ρ_1=8900 kg/m^3, ρ_2=8166 kg/m^3, E_1=205.098 GPa, E_2=207.788 GPa, ν_1=0.31, ν_2=0.317756).

	p=0		p=0.7		p=1		p=5		p=15	
	Present	Ref. [44]	Present	Ref. [44]	Present	Ref. [44]	Present	Ref. [44]	Present	Ref. [44]
n=1	13.548	13.548	13.269	13.269	13.211	13.211	12.998	12.998	12.933	12.933
n=2	4.5921	4.5920	4.4995	4.4994	4.4801	4.4800	4.4070	4.4068	4.3837	4.3834
n=3	4.2646	4.2633	4.1761	4.1749	4.1582	4.1569	4.0904	4.0891	4.0667	4.0653
n=4	7.2278	7.2250	7.0718	7.0691	7.0411	7.0384	6.9279	6.9251	6.8885	6.8856
n=5	11.547	11.542	11.295	11.290	11.245	11.241	11.065	11.061	11.003	10.999
n=6	16.904	16.897	16.533	16.527	16.461	16.455	16.198	16.192	16.108	16.101
n=7	23.253	23.244	22.743	22.735	22.643	22.635	22.282	22.273	22.158	22.148
n=8	30.584	30.573	29.913	29.903	29.782	29.771	29.307	29.296	29.144	29.132
n=9	38.895	38.881	38.041	38.028	37.875	37.862	37.270	37.257	37.063	37.048
n=10	48.185	48.168	47.126	47.111	46.920	46.905	46.171	46.155	45.915	45.897

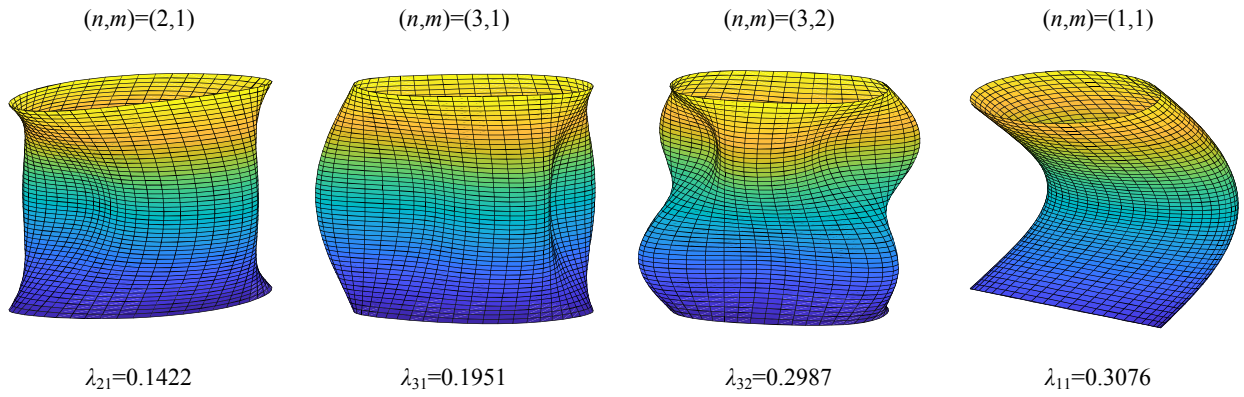

Fig. 5
Vibrational mode shapes associated with the first to fourth lowest natural frequencies of the shell.

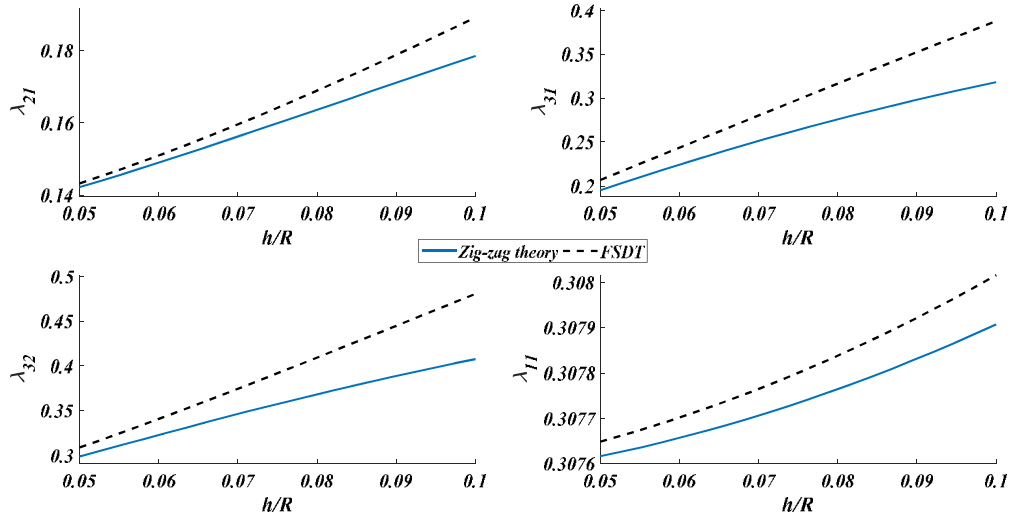

Fig. 6
The effects of the thickness-to-radius ratio on the natural frequencies of the shell.

Fig. 6 is presented to examine the effects of the thickness-to-radius ratio of the shell on the natural frequencies and the dependency of the natural frequencies on the employed shell theory. An increase in the thickness of the shell results in higher rigidity and mass which have opposite effects on the natural frequencies of the shell. However, by increasing the thickness of the shell the flexural rigidity of the shell experiences a higher increase in comparison with the mass. Thus, the natural frequencies increase in all vibrational modes as the thickness of the shell increases. This figure shows that the natural frequencies predicted based on the zig-zag theory are always lower than the natural frequencies predicted based on the FSDT. The main reason behind this can be explained by Fig. 3. As shown in this figure, utilizing the zig-zag theory provides more flexibility which reduces the rigidity of the shell and results in lower and more accurate natural frequencies. Fig. 6 shows that the differences between the natural frequencies predicated based on the zig-zag theory and the FSDT increase by increasing the thickness of the shell. It shows the importance of the zig-zag effect for thick sandwich structures.

For various types of FGM, Fig. 7 shows the effects of the material index in the FGAH core on the natural frequencies of the shell. According to Fig. 2, increases in the material indexes in the P-FGM and the E-FGM cores result in lower volume fractions of the ceramic. According to the material properties of Alumina (Al_2O_3) and Aluminum (Al), these reductions decrease both the mass and the rigidity of the shell that have opposite effects on the natural frequencies of the shell. Thus, depending on the vibrational mode, the material index has different effects on the natural frequencies of the shell which can be seen in Fig. 7. According to Fig. 2, it can be concluded that an increase in the material index in the S-FGM core reduces the volume fraction of the ceramic in the half of the shell and increase the volume fraction of the ceramic in the other half. Thus, as shown in Fig. 7, the material index has a weak effect on the natural frequencies of the sandwich shell with the S-FGM AH core. Fig. 7 also shows that for the same values of the material index, the natural frequencies of the sandwich shell with the P-FGM AH core are higher than the natural frequencies of the sandwich shell with the E-FGM AH core.

According to Fig. 7, the sandwich cylindrical shells with the P-FGM and the S-FGM core have the same natural frequencies for p=1. It can be explained by the variation of the material properties depicted in Fig. 2. Fig. 7 shows that for high values of the material index in the FGAH core ($p\to\infty$), the natural frequencies reach specified values. According to Eq. (1), for the P-FGM and the E-FGM, these values are the natural frequencies of a sandwich cylindrical shell with an AH core made of Aluminum. Also, for the S-FGM core, $p\to\infty$ means a sandwich cylindrical shell with an AH core in which half of the core is made of Aluminum and the other half is made of Alumina.

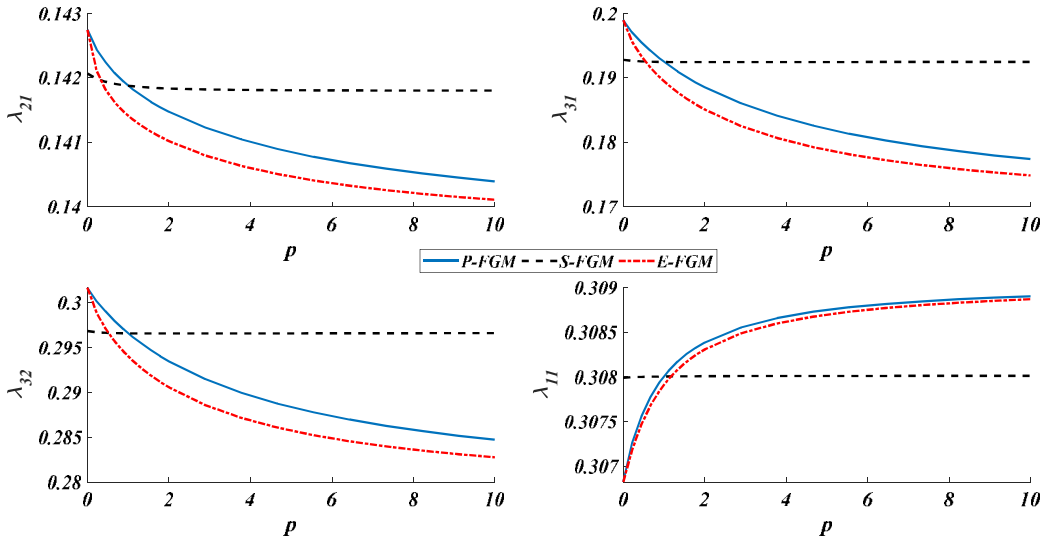

Fig. 7
The effects of the material gradation in the FGAH core on the natural frequencies of the shell.

For some selected values of the inclined angle and a specific value of the thickness of the shell, Fig. 8 shows the effects of the thickness of the FGAH core on the natural frequencies of the shell. In comparison with the isotropic homogenous face layers, the FGAH core benefits from lower density and has lower elastic and shear moduli. As a result, an increase in the thickness of the core brings about lower mass and rigidity which have opposite effects on the natural frequencies of the shell. Fig. 8 shows that as the thickness of the FGAH core increases, the natural frequencies experience an initial increase (due to the higher reduction in the mass) followed by a reduction (due to a higher decrease in the rigidity). In other words, for each vibrational mode, there is an optimal ratio between the thickness of the FGAH core and the thickness of the shell which provides the highest natural frequency.

Eq. (3) shows that the density of the FGAH core increases by increasing the inclined angle. The reason behind this is the increase in the number of cells in the FGAH core. It is shown in Ref. [28] that by variation of the inclined angle from zero to about 90°, the elastic and shear moduli experience different variations including decreases in some ones and increases in others. As shown in Fig. 8, as the inclined angle in the FGAH core increases from 15° to 60°, the natural frequencies decrease in all vibrational modes which can be explained by the increase in the density of the FGAH core.

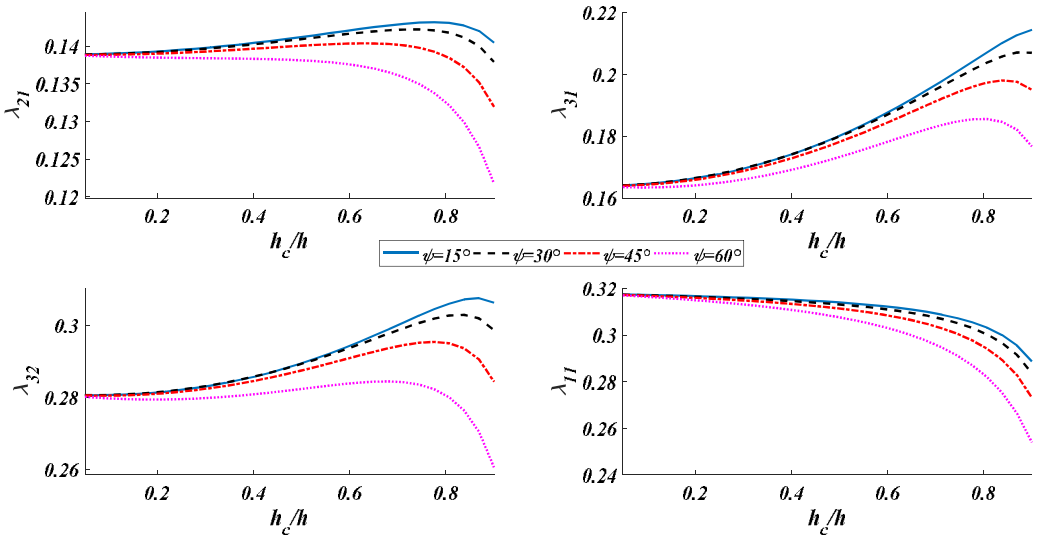

Fig. 8
The effects of the thickness of the FGAH core and the inclined angle on the natural frequencies of the shell.

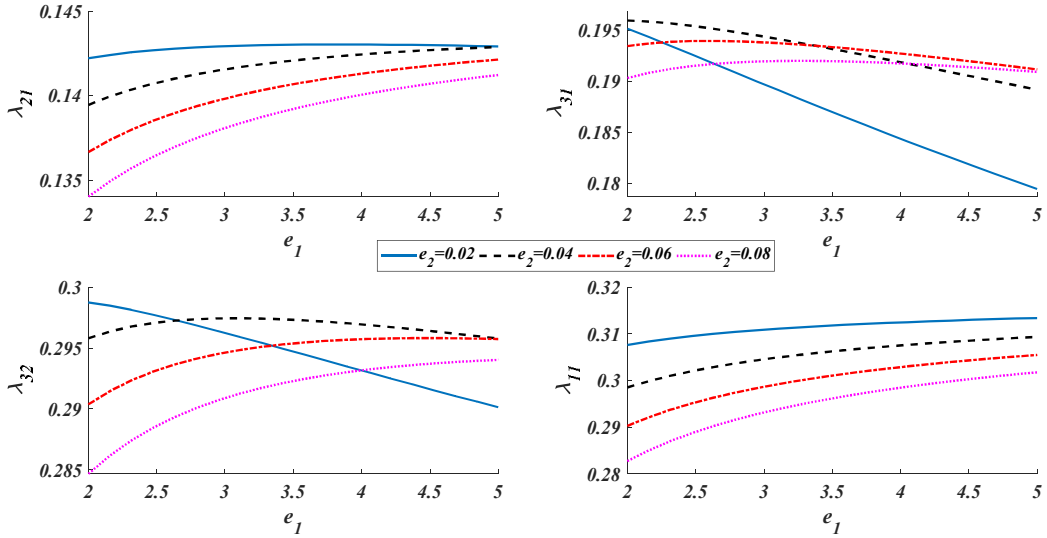

Fig. 9
The effects of the geometric parameters e_1 and e_2 in the FGAH core on the natural frequencies of the shell.

Fig. 9 is presented to study the effects of the geometric parameters e_1 and e_2 in the FGAH core on the natural frequencies of the shell. An increase in e_1 reduces the number of cells in the FGAH core which brings about lower density. As shown in Ref. [28], an increase in e_1 has different and opposite effects on the elastic and shear moduli of the FGSH core. Thus, as Fig. 9 shows, the natural frequencies experience different variations by increasing the geometric parameter e_1.

An increase in the geometric parameter e_2 means an increase in the thickness of the walls in the FGAH core. This increase brings about higher density and higher elastic and shear moduli of the FGAH core. Thus, by increasing the geometric parameter e_2 both the mass and the rigidity of the shell increase which have opposite effects on the natural frequencies of the shell. As a result, as shown in Fig. 9, the natural frequencies experience different variations by increasing the geometric parameter e_2.

5 CONCLUSIONS

A theoretical study was presented on the free vibration analysis of a sandwich cylindrical shell with a re-entrant FGAH core and isotropic homogenous face layers. It was assumed that the volume fraction of the ceramic phase in the FGAH core varies from zero at the inner surface of the core to one at the outer one according to various patterns including power-law, sigmoid, and exponential patterns. The sandwich shell was modeled based on the zig-zag theory, and an exact solution was presented via the Navier method to determine the natural frequencies of the shell with simply supported boundary conditions. The main findings of the presented paper can be stated as follows:

- The natural frequencies of the shell increase in all vibrational modes as the thickness of the shell increases.
- The natural frequencies predicted based on the zig-zag theory are lower than the natural frequencies predicted based on the FSDT.
- The differences between the natural frequencies predicated based on the zig-zag theory and the FSDT increase by increasing the thickness of the shell.
- For the P-FGM and the E-FGM cores, the material index has different effects on the natural frequencies of the shell. However, for the S-FGM core, the material index does not have a sensible effect on the natural frequencies of the shell.
- For the same values of the material index, the natural frequencies of the sandwich shell with the P-FGM AH core are higher than the natural frequencies of the sandwich shell with the E-FGM AH core.
- For a specific value of the thickness of the shell, by increasing the thickness of the FGAH core, the natural frequencies experience an initial increase followed by a reduction. In other words, for each vibrational mode, there is an optimal ratio between the thickness of the FGAH core and the thickness of the shell which brings about the highest natural frequency.
- For all vibrational modes, the natural frequencies decrease as the inclined angle in the FGAH core increases.
- Depending on the vibrational mode, the natural frequencies experience different variations by increasing the geometric parameters e_1 (aspect ratio in the cells) and e_2 (wall thickness of the cells).

REFERENCES

[1] A. Ghorbanpour Arani, M. Jamali, A.H. Ghorbanpour Arani, R. Kolahchi, M. Mosayyebi, Electro-magneto wave propagation analysis of viscoelastic sandwich nanoplates considering surface effects, *Proceedings of the Institution of Mechanical Engineers, Part C: Journal of Mechanical Engineering Science* 231(2) (2017) 387-403.

[2] E. Haghparast, A.A. Ghorbanpour Arani, A. Ghorbanpour Arani, Effect of fluid–structure interaction on vibration of moving sandwich plate with Balsa wood core and nanocomposite face sheets, *International Journal of Applied Mechanics* 12(07) (2020) 2050078.

[3] A.H. Ghorbanpour Arani, M. Abdollahian, A. Ghorbanpour Arani, Nonlinear dynamic analysis of temperature-dependent functionally graded magnetostrictive sandwich nanobeams using different beam theories, *Journal of the Brazilian Society of Mechanical Sciences and Engineering* 42 (2020) 1-20.

[4] A.A. Ghorbanpour Arani, Z. Khoddami Maraghi, A. Ghorbanpour Arani, The Frequency Response of Intelligent Composite Sandwich Plate Under Biaxial In-Plane Forces, *Journal of Solid Mechanics* 15(1) (2023).

[5] A.H. Ghorbanpour Arani, A. Rastgoo, M. Sharafi, R. Kolahchi, A. Ghorbanpour Arani, Nonlocal viscoelasticity based vibration of double viscoelastic piezoelectric nanobeam systems, *Meccanica* 51 (2016) 25-40.

[6] A.H. Ghorbanpour Arani, A. Rastgoo, A. Hafizi Bidgoli, R. Kolahchi, A. Ghorbanpour Arani, Wave propagation of coupled double-DWBNNTs conveying fluid-systems using different nonlocal surface piezoelasticity theories, *Mechanics of Advanced Materials and Structures* 24(14) (2017) 1159-1179.
[7] P. Sourani, A. Ghorbanpour Arani, M. Hashemian, S. Niknejad, Nonlinear dynamic stability analysis of CNTs reinforced piezoelectric viscoelastic composite nano/micro plate under multiple physical fields resting on smart foundation, *Proceedings of the Institution of Mechanical Engineers, Part C: Journal of Mechanical Engineering Science* 238(10) (2024) 4307-4342.
[8] A. Ghorbanpour Arani, N. Miralaei, A. Farazin, M. Mohammadimehr, An extensive review of the repair behavior of smart self-healing polymer matrix composites, *Journal of Materials Research* 38(3) (2023) 617-632.
[9] K. Torabi, H. Afshari, F. Hajiaboutalebi, Vibration and flutter analyses of cantilever trapezoidal honeycomb sandwich plates, *Journal of Sandwich Structures & Materials* 21(8) (2019) 2887-2920.
[10] S. Galehdari, H. Khodarahmi, A. Atrian, Design and analysis of graded honeycomb shock absorber for increasing the safety of passengers in armored vehicles exposed to mine explosion, *Journal of Solid Mechanics* 9(2) (2017) 370-383.
[11] H. Alikhani, S. Derakhshan, H. Khoramishad, Experimental and Numerical Investigations of the Effect of Impact Angle and Impactor Geometry on the High-Velocity Impact Response of Aluminum Honeycomb Structures, *Journal of Solid Mechanics* 14(4) (2022).
[12] T.D. Qing, C.Y. Zhi, Wave propagation in sandwich panel with auxetic core, *Journal of Solid Mechanics* 2(4) (2010) 393-402.
[13] N.D. Duc, K. Seung-Eock, P.H. Cong, N.T. Anh, N.D. Khoa, Dynamic response and vibration of composite double curved shallow shells with negative Poisson's ratio in auxetic honeycombs core layer on elastic foundations subjected to blast and damping loads, *International Journal of Mechanical Sciences* 133 (2017) 504-512.
[14] H. Eipakchi, F.M. Nasrekani, Vibrational behavior of composite cylindrical shells with auxetic honeycombs core layer subjected to a moving pressure, *Composite Structures* 254 (2020) 112847.
[15] N.V. Nguyen, H. Nguyen-Xuan, T.N. Nguyen, J. Kang, J. Lee, A comprehensive analysis of auxetic honeycomb sandwich plates with graphene nanoplatelets reinforcement, *Composite Structures* 259 (2021) 113213.
[16] P. Xiao, Z. Yifeng, S. Jie, S. Zheng, Global buckling analysis of composite honeycomb sandwich plate with negative Poisson's ratio (CHSP-NPR) using variational asymptotic equivalent model, *Composite Structures* 264 (2021) 113721.
[17] F. Xu, K. Yu, L. Hua, In-plane dynamic response and multi-objective optimization of negative Poisson's ratio (NPR) honeycomb structures with sinusoidal curve, *Composite Structures* 269 (2021) 114018.
[18] Q.-H. Pham, P.-C. Nguyen, T.T. Tran, Free vibration response of auxetic honeycomb sandwich plates using an improved higher-order ES-MITC3 element and artificial neural network, *Thin-Walled Structures* 175 (2022) 109203.
[19] T.Q. Quan, V.M. Anh, V. Mahesh, N.D. Duc, Vibration and nonlinear dynamic response of imperfect sandwich piezoelectric auxetic plate, *Mechanics of Advanced Materials and Structures* 29(1) (2022) 127-137.
[20] N.D. Dat, T.Q. Quan, N.D. Duc, Vibration analysis of auxetic laminated plate with magneto-electro-elastic face sheets subjected to blast loading, *Composite Structures* 280 (2022) 114925.
[21] Y. Li, B. Liu, Thermal buckling and free vibration of viscoelastic functionally graded sandwich shells with tunable auxetic honeycomb core, *Applied Mathematical Modelling* 108 (2022) 685-700.
[22] A. Pakrooyan, P. Yousefi, K. Khorshidi, M.M. Najafizadeh, A. Nezamabadi, Free vibration analysis of an auxetic honeycomb sandwich plate placed at the wall of a fluid tank, *Ocean Engineering* 263 (2022) 112353.
[23] P.H. Cong, V.D. Trung, N.D. Khoa, N.D. Duc, Vibration and nonlinear dynamic response of temperature-dependent FG-CNTRC laminated double curved shallow shell with positive and negative Poisson's ratio, *Thin-Walled Structures* 171 (2022) 108713.
[24] B. Liu, S. Li, Y. Li, Bending of FGM sandwich plates with tunable auxetic core using DQM, *European Journal of Mechanics-A/Solids* 97 (2023) 104838.
[25] S. Sadikbasha, V. Pandurangan, Crashworthiness of auxetic hexachiral core under in-plane loading, *Materials Today: Proceedings* (2023).
[26] B. Nečemer, Ž. Božić, S. Glodež, Fatigue resistance of the auxetic honeycombs, *Procedia Structural Integrity* 46 (2023) 68-73.
[27] M. Rai, A. Chawla, S. Mukherjee, Parametric study of re-entrant honeycomb cored auxetic sandwich panel exposed to blast loading, *Materials Today: Proceedings* (2023).
[28] M. Sarafraz, H. Seidi, F. Kakavand, N.S. Viliani, Free vibration and buckling analyses of a rectangular sandwich plate with an auxetic honeycomb core and laminated three-phase polymer/GNP/fiber face sheets, *Thin-Walled Structures* 183 (2023) 110331.
[29] M. Sarafraz, H. Seidi, F. Kakavand, N.S. Viliani, Flutter characteristics of a rectangular sandwich plate with laminated three-phase polymer/GNP/fiber face sheets and an auxetic honeycomb core in yawed supersonic fluid flow, *Journal of the Brazilian Society of Mechanical Sciences and Engineering* 45(4) (2023) 197.
[30] M. Koizumi, The concept of FGM, *Ceramic transactions* 34 (1993) 3-10.
[31] J.-h. Zhang, B.-j. Dong, B. He, Y. Sun, Free vibrations and impact resistance of a functionally graded honeycomb sandwich plate, *Shock and Vibration* 2021 (2021) 1-15.
[32] F. Li, W. Yuan, C. Zhang, Free vibration and sound insulation of functionally graded honeycomb sandwich plates, *Journal of Sandwich Structures & Materials* 24(1) (2022) 565-600.

[33] H. Amirabadi, A. Darakhsh, M. Sarafraz, H. Afshari, Vibration characteristics of a cylindrical sandwich shell with an FG auxetic honeycomb core and nanocomposite face layers subjected to supersonic fluid flow, *Noise & Vibration Worldwide* (2024) 09574565241252994.
[34] H. Amirabadi, A. Mottaghi, M. Sarafraz, H. Afshari, Free vibrational behavior of a conical sandwich shell with a functionally graded auxetic honeycomb core, *Journal of Vibration and Control* (2024) 10775463241240215.
[35] X. Zhu, J. Zhang, W. Zhang, J. Chen, Vibration frequencies and energies of an auxetic honeycomb sandwich plate, *Mechanics of Advanced Materials and Structures* 26(23) (2019) 1951-1957.
[36] H. Murakami, Laminated composite plate theory with improved in-plane responses, (1986).
[37] A. Ghorbanpour Arani, F. Kiani, H. Afshari, Free and forced vibration analysis of laminated functionally graded CNT-reinforced composite cylindrical panels, *Journal of Sandwich Structures & Materials* 23(1) (2021) 255-278.
[38] A. Ghorbanpour Arani, F. Kiani, H. Afshari, Aeroelastic analysis of laminated FG-CNTRC cylindrical panels under yawed supersonic flow, *International Journal of Applied Mechanics* 11(06) (2019) 1950052.
[39] J.N. Reddy, Mechanics of laminated composite plates and shells: theory and analysis, *CRC press* 2003.
[40] V. Mohammadlou, Z. Khoddami Maraghi, A. Ghorbanpour Arani, Thermoelastic analysis of axisymmetric conical shells: Investigating stress–strain response under uniform heat flow with semi-coupled approach, *Numerical Heat Transfer, Part A: Applications* (2024) 1-22.
[41] J.N. Reddy, Energy principles and variational methods in applied mechanics, *John Wiley & Sons* 2017.
[42] A. Ghorbanpour Arani, E. Haghparast, A.H. Ghorbanpour Arani, Size□dependent vibration of double□bonded carbon nanotube□reinforced composite microtubes conveying fluid under longitudinal magnetic field, *Polymer Composites* 37(5) (2016) 1375-1383.
[43] H. Li, K.-Y. Lam, T.-Y. Ng, Rotating shell dynamics, *Elsevier* 2005.
[44] C. Loy, K. Lam, J. Reddy, Vibration of functionally graded cylindrical shells, *International Journal of Mechanical Sciences* 41(3) (1999) 309-324.